Anal. Chem. **2010,** *82,* 2204–2212

Ac Dielectrophoresis of Tin Oxide Nanobelts Suspended in Ethanol: Manipulation and Visualization

Surajit Kumar,*,† Zhengchun Peng,† Heungjoo Shin,‡ Zhong Lin Wang,§ and Peter J. Hesketh†

George W. Woodruff School of Mechanical Engineering and School of Materials Science and Engineering, Georgia Institute of Technology, Atlanta, Georgia 30332, and School of Mechanical and Advanced Materials Engineering, Ulsan National Institute of Science and Technology (UNIST), Banyeon-ri 100, Ulsan 689-798, Korea

This article presents results of detailed and direct real-time observations of the wide variety of SnO_2 nanobelt motions induced by ac dielectrophoresis (DEP) in an innovative microfluidic setup. High ac electric fields were generated on a gold microelectrode (~20 μm electrode gap) array, patterned on a glass substrate and covered by a ~10 μm tall polydimethylsiloxane (PDMS) microchannel. Ethanol suspended SnO_2 nanobelts were introduced into the microchannel, and the DEP experiments were performed. Negative DEP (repulsion) of the nanobelts was observed in the low-frequency range (<100 kHz) of the applied electric field, which caused rigid body motion as well as deformation of the nanobelts. The negative DEP effect observed in ethanol is unusual and contrary to what is predicted by the Clausius−Mossotti factor (using bulk SnO_2 conductivity and permittivity values) of the dipole approximation theory. In the high-frequency range (~1−10 MHz), positive DEP (attraction) of the nanobelts was observed. Pearl chain formation involving short nanobelts and particles was also observed in the two DEP regimes.

Nanobelts[1] are a new class of semiconducting metal oxide nanowires. The ribbonlike nanobelts are chemically pure and predominantly single crystalline structures[1] formed by oxides (SnO_2, ZnO, In_2O_3, $SrTiO_3$, etc.) and other materials (ZnSe, ZnS, Zn_3P_2, Cd_3P_2, CdS, InN, etc.). They are structurally uniform with clean, sharp, smooth surfaces and have rectangular cross sections.[1] Nanobelts have great potential as building blocks for nanoscale devices. Examples of the diverse application potentials of the novel nanobelts that have been demonstrated so far include SnO_2 nanobelt sensors for the detection of nerve agent stimulant,[2] hydrogen[3] (at room-temperature), and other gases;[4,5] pH sensor;[6] thermal sensor and switch based on a plasma polymer/ZnO suspended nanobelt bimorph structure;[7] field effect transistors (FETs) based on SnO_2,[8] ZnO,[8] Zn_3P_2,[9] Cd_3P_2,[9] and CdS[10] nanobelts; ZnO,[11] and ZnS[12] nanobelts as field emitters; CdS nanobelt based optical switches[13] and ZnSe nanobelt based blue/ultraviolet light-sensitive photodetectors;[14] ZnO nanobelt waveguide;[15] InN nanobelt based infrared laser[16] and CdSe nanobelt based red-color emitting laser;[17] ZnO nanobelt acoustic resonator;[18] nanobelts used as nanocantilevers;[19] and finally the possibility of exploiting nanobelts with magnetic properties.[20] There is a growing need for studying methods for the manipulation of nanobelts and other types of nanostructures to assemble them into nanodevices for useful applications. Some of the manipulation methods reported in the literature include fluid flow alignment of nanowires[21] and carbon

* Corresponding author. E-mail: surajitk@gatech.edu. Fax: 404-894-8496.
† George W. Woodruff School of Mechanical Engineering.
‡ Ulsan National Institute of Science and Technology.
§ School of Materials Science and Engineering.

(1) Pan, Z. W.; Dai, Z. R.; Wang, Z. L. *Science* **2001**, *291*, 1947–1949.
(2) Yu, C.; Hao, Q.; Saha, S.; Shi, L.; Kong, X.; Wang, Z. L. *Appl. Phys. Lett.* **2005**, *86*, 063101-1-3.
(3) Fields, L. L.; Zheng, J. P.; Cheng, Y.; Xiong, P. *Appl. Phys. Lett.* **2006**, *88*, 263102-1-3.
(4) Comini, E.; Faglia, G.; Sberveglieri, G.; Pan, Z.; Wang, Z. L. *Appl. Phys. Lett.* **2002**, *81*, 1869–1872.
(5) Comini, E.; Faglia, G.; Sberveglieri, G.; Calestani, D.; Zanotti, L.; Zha, M. *Sens. Actuators, B* **2005**, *111−112*, 2–6.
(6) Cheng, Y.; Xiong, P.; Yun, C. S.; Strouse, G. F.; Zheng, J. P.; Yang, R. S.; Wang, Z. L. *Nano Lett.* **2008**, *8*, 4179–4184.
(7) He, J. H.; Singamaneni, S.; Ho, C. H.; Lin, Y. H.; McConney, M. E.; Tsukruk, V. V. *Nanotechnology* **2009**, *20*, 065502-1-5.
(8) Arnold, M.; Avouris, P.; Pan, Z. W.; Wang, Z. L. *J. Phys. Chem. B* **2003**, *107*, 659–663.
(9) Shen, G.; Chen, P. C.; Bando, Y.; Golberg, D.; Zhou, C. *Chem. Mater.* **2008**, *20*, 7319–7323.
(10) Ma, R. M.; Dai, L.; Huo, H. B.; Yang, W. Q.; Qin, G. G.; Tan, P. H.; Huang, C. H.; Zheng, J. *Appl. Phys. Lett.* **2006**, *89*, 203120-1-3.
(11) Wang, W. Z.; Zeng, B. Q.; Yang, J.; Poudel, B.; Huang, J. Y.; Naughton, M. J.; Ren, Z. F. *Adv. Mater.* **2006**, *18*, 3275–3278.
(12) Fang, X. S.; Bando, Y.; Shen, G. Z.; Ye, C. H.; Gautam, U. K.; Costa, P. M. F. J.; Zhi, C. Y.; Tang, C. C.; Golberg, D. *Adv. Mater.* **2007**, *19*, 2593–2596.
(13) Gao, T.; Li, Q. H.; Wang, T. H. *Appl. Phys. Lett.* **2005**, *86*, 173105-1-3.
(14) Fang, X. S.; Xiong, S. L.; Zhai, T. Y.; Bando, Y.; Liao, M.; Gautam, U. K.; Koide, Y.; Zhang, X. G.; Qian, Y.; Golberg, D. *Adv. Mater.* **2009**, *21*, 5016–5021.
(15) Xu, X.; Brossard, F. S. F.; Williams, D. A.; Collins, D. P.; Holmes, M. J.; Taylor, R. A.; Zhang, X. *Appl. Phys. Lett.* **2009**, *94*, 231103-1-3.
(16) Hu, M. S.; Hsu, G. M.; Chen, K. H.; Yu, C. J.; Hsu, H. C.; Chen, L. C.; Hwang, J. S.; Hong, L. S.; Chen, Y. F. *Appl. Phys. Lett.* **2007**, *90*, 123109-1-3.
(17) Pan, A.; Liu, R.; Zhang, Q.; Wan, Q.; He, P.; Zacharias, M.; Zou, B. *J. Phys. Chem. C* **2007**, *111*, 14253–14256.
(18) Buchine, B. A.; Hughes, W. L.; Degertekin, F. L.; Wang, Z. L. *Nano Lett.* **2006**, *6*, 1155–1159.
(19) Hughes, W. L.; Wang, Z. L. *Appl. Phys. Lett.* **2003**, *82*, 2886–2888.
(20) Xu, C. X.; Sun, X. W.; Dong, Z. L.; Yu, M. B.; Xiong, Y. Z.; Chen, J. S. *Appl. Phys. Lett.* **2005**, *86*, 173110-1-3.
(21) Huang, Y.; Duan, X.; Wei, Q.; Lieber, C. M. *Science* **2001**, *291*, 630–633.

10.1021/ac901287z © 2010 American Chemical Society
Published on Web 02/12/2010

nanotubes;[22−24] assembly and manipulation of nanotubes[25] and nanorods[26] using atomic force microscopes (AFM); application of dc electric field for aligning single-walled carbon nanotubes (SWNTs);[27] electrophoresis of $Mo_6S_3I_6$ nanowires;[28] and dielectrophoresis (DEP)[29,30] based assembly[31] of nanostructures. While traditionally DEP has commonly been used in the manipulation of biological cells and macromolecules,[32] recently this technique has become popular for the manipulation of nanostructures.[31] Ac dielectrophoretic alignment and assembly has been demonstrated in metallic (Au) nanowires,[33] semiconducting nanowires,[34] metal oxide nanowires,[35] nickel silicate nanowires,[36] multiwalled carbon nanotubes (MWNTs),[37,38] and SWNTs.[39−42] Alignment of MWNTs using a dc field has also been reported.[43] However, these reports are mostly limited to attracting the nanostructures between electrodes for device fabrication, including our prior work on SnO_2 nanobelts,[44] without real-time monitoring of the details of the motion and observation of change in position and shape.

A very limited number of real-time nanowire assembly studies have been published in the literature so far. Fan et al.[45] and Papadakos et al.[46] studied the real-time motion of gold (Au) nanowires under the action of ac dielectrophoretic forces, and Wissner-Gross[47] studied real-time assembly, reconfiguration, and disassembly using P-type silicon nanowires suspended in benzyl alcohol. Hammers et al.[48] and Marcus et al.[49] performed real-time detection of nanowire bridging events in aqueous media using gold (Au) nanowires, silicon nanowires, and carbon nanofibers. The present work reports the experimental results of detailed real-time observation of individual SnO_2 nanobelts moving under the influence of ac dielectrophoretic forces generated in ethanol medium. Depending on the applied electric field frequency, the experiments revealed a wide variety of nanobelt motions and novel DEP behavior in the SnO_2/ethanol system.

THEORY

The application of electric fields to a suspension of particles can generate forces on both the particle and the fluid depending on their properties. Electroosmosis[30] occurs if there is a gradient in charge density in the fluid. This phenomenon is not significant in insulating liquids since the presence of electrical double layers is unlikely. Electrothermally driven fluid flows[30] occur if there is a temperature gradient in the fluid. The forces generated by electric fields on particles are generally due to dielectrophoresis, and the effects of electrophoresis can also be included if electric charge is present on them.[30] While in theory all the different types of forces can be present in an electrokinetic system, in practice only a few are important depending on the details of the situation. Using the order of magnitude analysis described by Liu et al.[50] for estimation of the various forces on nanowires in an electrokinetic system it is found that in the case of DEP of SnO_2 nanobelts suspended in ethanol, ac electroosmotic flow, buoyancy, electrothermal effects, and Brownian motion can safely be ignored.

Dielectrophoresis (DEP)[29,30] is a phenomenon in which force is induced due to the influence of a nonuniform electric field on a polarizable particle suspended in a liquid medium, often causing the particle to move. Using the dipole approximation,[29,30] it has been shown that for a homogeneous spherical particle of radius R, suspended in a fluid medium, the time-averaged DEP force $\boldsymbol{F}_{\mathbf{dep}}$, on the particle subjected to a local electric field $\boldsymbol{E}$ (phasor amplitude), of angular frequency ω, when the ac electric field magnitude is varying with location but the phase is constant, is given by[30]

$$\boldsymbol{F}_{\mathbf{dep}} = \pi\varepsilon_m R^3 \,\mathrm{Re}(\tilde{f}_{CM})\nabla|\boldsymbol{E}|^2 = 2\pi\varepsilon_m R^3 \,\mathrm{Re}(\tilde{f}_{CM})\nabla|\boldsymbol{E}_{\mathbf{rms}}|^2 \quad (1)$$

where $\boldsymbol{E}_{\mathbf{rms}}$ is the root-mean-square (rms) value of the electric field. $\tilde{f}_{CM}$ is known as the Clausius−Mossotti factor expressed by

$$\tilde{f}_{CM} = \left(\frac{\tilde{\varepsilon}_p - \tilde{\varepsilon}_m}{\tilde{\varepsilon}_p + 2\tilde{\varepsilon}_m}\right) \quad (2)$$

(22) Yan, Y. H.; Li, S.; Chen, L. Q.; Chan-Park, M. B.; Zhang, Q. *Nanotechnology* **2006**, *17*, 5696–5701.
(23) Li, S.; Liu, N.; Chan-Park, M. B.; Yan, Y.; Zhang, Q. *Nanotechnology* **2007**, *18*, 455302-1-7.
(24) Li, J. Q.; Zhang, Q.; Yan, Y. H.; Li, S.; Chen, L. Q. *IEEE Trans. Nanotechnol.* **2007**, *6*, 481–484.
(25) Hertel, T.; Martel, R.; Avouris, P. *J. Phys. Chem. B* **1998**, *102*, 910–915.
(26) Hsieh, S.; Meltzer, S.; Wang, C. R. C.; Requicha, A. A. G.; Thompson, M. E.; Koel, B. E. *J. Phys. Chem. B* **2002**, *106*, 231–234.
(27) Kumar, M. S.; Lee, S. H.; Kim, T. Y.; Kim, T. H.; Song, S. M.; Yang, J. W.; Nahm, K. S.; Suh, E. K. *Solid-State Electron.* **2003**, *47*, 2075–2080.
(28) Ploscaru, M.; Mrzel, A.; Vrbanic, D.; Umek, P.; Uplaznik, M.; Podobnik, B.; Mihailovic, D.; Vengust, D.; Nemanic, V.; Zumer, M.; Zajec, B. *AIP Conf. Proc.* **2004**, *723*, 435–438.
(29) Pethig, R. *Dielectric and Electronic Properties of Biological Materials*; John Wiley & Sons: Chichester, U.K., 1979.
(30) Morgan, H.; Green, N. G. *AC Electrokinetic: Colloids and Nanoparticles*; Research Studies Press: Baldock, Hertfordshire, U.K., 2003.
(31) Burke, P. J. In *Encyclopedia of Nanoscience and Nanotechnology*, Vol. 6; Nalwa, H. S., Ed.; American Scientific Publishers: Stevenson Ranch, CA, 2004; pp 623−641.
(32) Voldman, J. *Annu. Rev. Biomed. Eng.* **2006**, *8*, 425–454.
(33) Smith, P. A.; Nordquist, C. D.; Jackson, T. N.; Mayer, T. S.; Martin, B. R.; Mbindyo, J.; Mallouk, T. E. *Appl. Phys. Lett.* **2000**, *77*, 1399–1401.
(34) Duan, X.; Huang, Y.; Cui, Y.; Wang, J.; Lieber, C. M. *Nature* **2001**, *409*, 66–69.
(35) Wang, D.; Zhu, R.; Zhou, Z.; Ye, X. *Appl. Phys. Lett.* **2007**, *90*, 103110-1-3.
(36) Dong, L. F.; Bush, J.; Chirayos, V.; Solanki, R.; Jiao, J. *Nano Lett.* **2005**, *5*, 2112–2115.
(37) Yamamoto, K.; Akita, S.; Nakayama, Y. *J. Phys. D: Appl. Phys.* **1998**, *31*, L34–L36.
(38) Suehiro, J.; Zhou, G.; Hara, M. *J. Phys. D: Appl. Phys.* **2003**, *36*, L109–L114.
(39) Chen, X. Q.; Saito, T.; Yamada, H.; Matsushige, K. *Appl. Phys. Lett.* **2001**, *78*, 3714–3716.
(40) Krupke, R.; Hennrich, F.; Beckmann, H. B.; Hampe, O.; Malik, S.; Kappes, M. M.; Lohneysen, H. V. *Appl. Phys. A: Mater. Sci. Process.* **2003**, *76*, 397–400.
(41) Chung, J.; Lee, J. *Sens. Actuators, A* **2003**, *104*, 229–235.
(42) Nagahara, L. A.; Amlani, I.; Lewenstein, J.; Tsui, R. K. *Appl. Phys. Lett.* **2002**, *80*, 3826–3828.
(43) Yamamoto, K.; Akita, S.; Nakayama, Y. *Jpn. J. Appl. Phys.* **1996**, *35*, L917–L918.
(44) Kumar, S.; Rajaraman, S.; Gerhardt, R. A.; Wang, Z. L.; Hesketh, P. J. *Electrochim. Acta* **2005**, *51*, 943–951.
(45) Fan, D. L.; Zhu, F. Q.; Cammarata, R. C.; Chien, C. L. *Appl. Phys. Lett.* **2004**, *85*, 4175–4177.
(46) Papadakis, S. J.; Gu, Z.; Gracias, D. H. *Appl. Phys. Lett.* **2006**, *88*, 233118-1-3.
(47) Wissner-Gross, A. D. *Nanotechnology* **2006**, *17*, 4986–4990.
(48) Hamers, R. J.; Beck, J. D.; Eriksson, M. A.; Li, B.; Marcus, M. S.; Shang, L.; Simmons, J.; Streifer, J. A. *Nanotechnology* **2006**, *17*, S280–S286.
(49) Marcus, M. S.; Shang, L.; Li, B.; Streifer, J. A.; Beck, J. D.; Perkins, E.; Eriksson, M. A.; Hamers, R. J. *Small* **2007**, *3*, 1610–1617.
(50) Liu, Y.; Chung, J. H.; Liu, W. K.; Ruoff, R. S. *J. Phys. Chem. B* **2006**, *110*, 14098–14106.

where $\tilde{\varepsilon}_p = \varepsilon_p - j(\sigma_p/\omega)$ is the complex permittivity of the particle, and $\tilde{\varepsilon}_m = \varepsilon_m - j(\sigma_m/\omega)$ is the complex permittivity of the fluid medium. ε_p and ε_m are the permittivities of the particle and the fluid medium, respectively. σ_p, and σ_m are the electrical conductivities of the particle and the fluid medium, respectively. Analogous expressions have also been derived for ellipsoidal particles.[30]

From the force expression, one can note that the frequency dependence of the DEP force is determined by the real part of the Clausius−Mossotti factor $\mathrm{Re}(\tilde{f}_{CM})$. It determines both the magnitude and the sign of the DEP force. The value of the $\mathrm{Re}(\tilde{f}_{CM})$ factor ranges from −0.5 to + 1.0 and can be calculated from the properties of the particle and the medium. If the value of $\mathrm{Re}(\tilde{f}_{CM})$ is positive, the particle moves toward higher electric field regions, and this phenomenon is termed as positive DEP (pDEP). If the value of $\mathrm{Re}(\tilde{f}_{CM})$ is negative, the particle moves toward lower electric field regions, and this phenomenon is termed as negative DEP (nDEP). Positive DEP occurs when the particle is more polarizable than the medium. The reverse is true for negative DEP.

For spherical particles, the limiting values of the real part of the Clausius−Mossotti factor at low and high frequencies are given by[30]

$$\omega \to 0, \quad \mathrm{Re}(\tilde{f}_{CM}) \to \frac{(\sigma_p - \sigma_m)}{(\sigma_p + 2\sigma_m)} \tag{3}$$

$$\omega \to \infty, \quad \mathrm{Re}(\tilde{f}_{CM}) \to \frac{(\varepsilon_p - \varepsilon_m)}{(\varepsilon_p + 2\varepsilon_m)} \tag{4}$$

The expressions indicate that the low-frequency limiting value depends on the conductivity mismatch, while the high-frequency limiting value depends on the permittivity mismatch of the particle and the suspending liquid medium.[30] However, for nonspherical particle shapes, the low- and high-frequency limiting values of the Clausius−Mossotti factor depend on the particular analytical model used,[51] and numerical simulations become necessary for accurate evaluation of the DEP characteristics in the case of particles with arbitrary shapes.

In general, the dipole approximation does not apply quantitatively to long objects like nanobelts and nanowires, since the different locations along a long object come under the influence of different magnitudes of electric field and field gradients. However, the Clausius−Mossotti factor can provide useful qualitative information on whether positive or negative DEP will occur in particular material and fluid combinations and in predicting the trends as a function of the electric field frequency. By extending the dipole approximation model in the case of ellipsoidal particles,[52] some simplified expressions have been derived and reported in the literature for DEP of long objects, such as nanowires and nanotubes. While such models may be used for qualitative purposes, their utility is still limited because they are valid only for very special cases of the object orientations. Also, such models are unlikely to be useful for calculating DEP forces in the case of nanobelts because of their unique shape and aspect ratio.[1] For accurate quantitative information full electrostatics calculations have to be performed numerically using methods such as the Maxwell stress tensor (MST) methodology.[53] Numerical simulations using this approach have been performed,[54] and the results are qualitatively similar to what is predicted by the simple dipole approximation model. However, because of space limitations those results are not discussed in this report. Hence, the Clausius−Mossotti factor of a spherical particle is still useful in predicting the qualitative DEP behavior of nanobelts while not being quantitatively accurate.

EXPERIMENTAL SECTION

The DEP manipulation of single nanobelts was carried out on linear arrays of gold (Au) microelectrodes, defined on Pyrex glass substrates. The microelectrode array was covered with a shallow (~10 μm tall, ~100 μm wide) PDMS (polydimethylsiloxane) microchannel so that the nanobelt suspension could be introduced in it.

Fabrication of Microchannel Mold Using SU-8 Resist. The microchannels were fabricated using replica molding of PDMS on SU-8 negative resist pattern. Figure 1a shows a schematic of the PDMS microchannel. The entrance region width is 250 μm, and the central region of the microchannel is 100 μm wide. The SU-8 mold was fabricated in two photolithography steps using two different types of negative resists. Two photomasks were designed with proper dimensions. For the first photolithography step, SU-8 2010 resist (MicroChem Corp., Newton, MA) was spun at 3000 rpm, with an initial acceleration of 500 rpm/s for a total of 40 s to obtain ~10 μm thickness on a silicon wafer. It was then soft baked at 95 °C. With the use of the first photomask, the resist layer on the wafer was exposed to UV radiation (365 nm wavelength) for a total energy of 160 mJ/cm^2. After postexposure hard bake at 95 °C, the wafer was developed in SU-8 developer (MicroChem Corp., Newton, MA) for ~5 min, rinsed with isopropyl alcohol, and dried using nitrogen. For the second photolithography step, SU-8 2075 resist (MicroChem Corp., Newton, MA) was spun at 800 rpm, with an initial acceleration of 400 rpm/s for a total of 40 s to obtain a ~250 μm thickness over the substrate with the first layer. Soft bake was performed at 95 °C. Alignment using the second photomask was performed, and UV radiation (365 nm wavelength) exposure was done for a total energy of 700 mJ/cm^2. After postexposure hard bake at 95 °C, the wafer was develop in SU-8 developer for ~60 min, rinsed with isopropyl alcohol, and dried in nitrogen. Figure 1b shows the resulting SU-8 mold, which was subsequently used for the replica molding of PDMS microchannels.

Replica Molding of PDMS Microchannels. PDMS (polydimethylsiloxane) polymer was prepared by adding Sylgard 184 Silicone Elastomer (Dow Corning Corporation, Midland, MI) curing agent to the base in a 1:10 ratio by weight. The mixture was degassed in a vacuum chamber for 30 min. The PDMS was then poured into the SU-8 mold wafer and thermally cured in an oven at 80 °C for 2 h. After the curing process, the cured PDMS layer was carefully peeled off from the mold wafer. The peeled PDMS layer was then cut carefully to obtain individual pieces (see

(51) Green, N. G.; Jones, T. B. *J. Phys. D: Appl. Phys.* **2007**, *40*, 78–85.
(52) Morgan, H.; Green, N. G. *J. Electrost.* **1997**, *42*, 279–293.
(53) Xujing, W.; Wang, X. B.; Gascoyne, P. R. C. *J. Electrost.* **1997**, *39*, 277–295.
(54) Kumar, S. Fluidic and Dielectrophoretic Manipulation of Tin Oxide Nanobelts. Ph.D. Dissertation, The Georgia Institute of Technology, Atlanta, GA, August 2008.

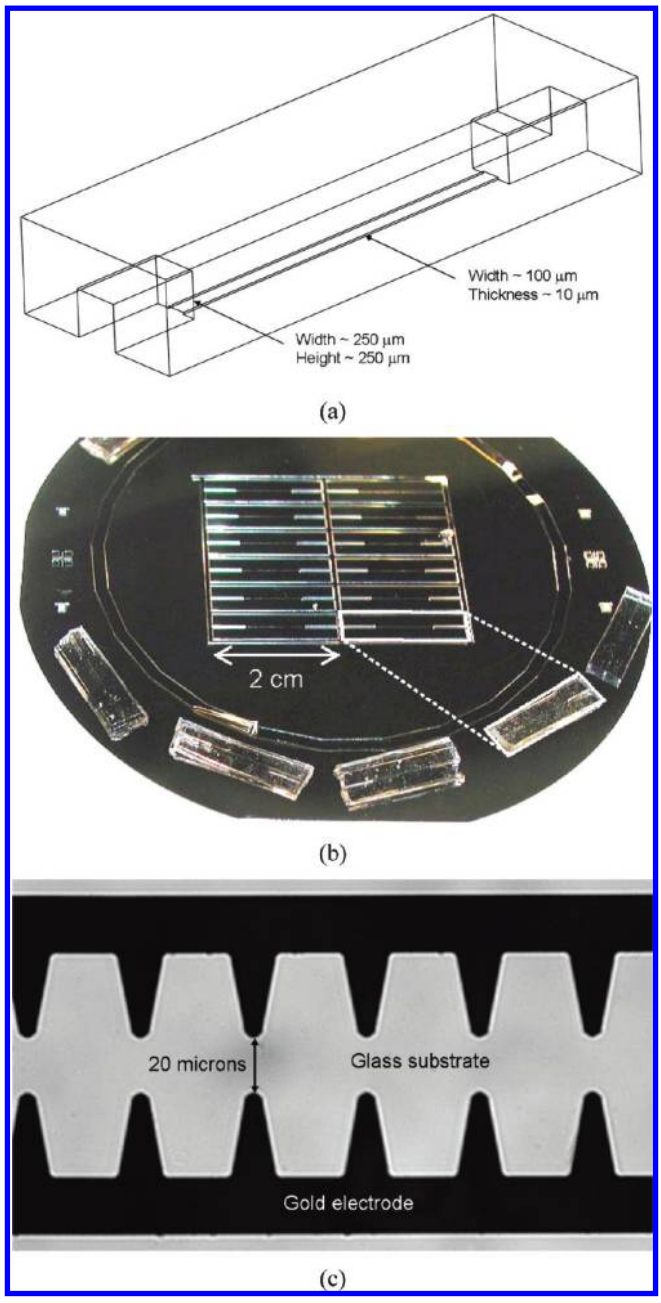

Figure 1. (a) Schematic showing structure of the PDMS microchannel that was fabricated using replica molding of SU-8 mold, (b) photograph showing an array (12 microchannels can be molded in a single batch) of SU-8 mold structures (seem in the central part of the wafer). After the molding process, the cured PDMS layer was peeled off from the SU-8 mold and individual pieces of the PDMS microchannels were cut (seen placed around the wafer periphery) for use in the DEP experiments, (c) optical microscope image of triangular gold microelectrodes (dark regions) fabricated on glass substrate (light regions).

the periphery of the mold wafer in Figure 1b), which contains the microchannels.

Microelectrode Fabrication. Fabrication of the DEP microelectrodes was carried out on a 500 μm thick Pyrex glass wafer (G.M. Associates Inc., Oakland, CA). The Ti/Au electrode was patterned on the wafer using standard lithographic techniques and the lift-off process. First, the pattern was defined in negative acting NR5-8000 photoresist (Futurrex Inc., Franklin, NJ). A 20 nm thick titanium (Ti) adhesion layer and a 250 nm thick gold (Au) layer were deposited using an electron beam evaporator system. The sample was then dipped in acetone for about 10 min to remove the photoresist. One of the electrode patterns is shown in Figure 1c, which consists of two linear arrays of triangular electrodes (minimum electrode gap ~20 μm) facing each other. The array of microelectrodes was connected to bond pads through wider gold (Au) lines which were also patterned during the photolithography and metal deposition step. Electrical connections to the bond pads were made using gold wires and conductive silver epoxy (Loctite 3880, Henkel Consumer Adhesives, Avon, OH). A layer of epoxy (Loctite Extra Time, Henkel Consumer Adhesives, Avon, OH) was then coated on the wire bonds to prevent them from breaking off.

SnO_2 Nanobelt Sample. SnO_2 nanobelt samples were made using the thermal evaporation (PVD) method outlined in previous reports.[1,55] It is a process in which condensed powder source material is vaporized at an elevated temperature in a tube furnace and the resultant vapor is condensed under controlled conditions (temperature, pressure, carrier gas atmosphere, substrate, etc.) to form the desired product. Argon (Ar) carrier gas entered an alumina tube in a furnace (50 cm long, 4 cm diameter), which was then pumped out by a rotary pump. The source material (SnO powder) was loaded on an alumina boat and positioned at the center of the tube. Several alumina plates (60 mm × 10 mm) were placed downstream, one behind the other, inside the alumina tube, which acted as substrates for collecting the growth products. At a pressure of 200−600 Torr, thermal evaporation of the SnO powder (purity 99.9%, melting point 1080 °C, Alfa Aesar, Ward Hill, MA) was carried out at ~1050 °C for 2 h, under an argon carrier gas flow of 50 sccm. The substrate temperature was carefully controlled during the deposition.

The nanobelt product obtained from the furnace was in the form of agglomerates, with the individual nanobelts intertwined with one another. The nanobelts were rectangular in cross section, had widths of 30−300 nm, had width-to-thickness ratios of 5−10, and were up to a few millimeters long.[1] Sometimes, nanobelts wider than 300 nm were also encountered in the samples. While the size range is determined by the growth conditions,[1,55] there is still a wide variation and distribution in the nanobelt sizes for any particular batch of growth product. In addition to the nanobelts, the sample also contained smaller amounts of other structures, such as nanodisks[55] and particles. In order to use the nanobelts in the DEP experiments, it was necessary to separate the agglomerates into individual nanobelts of shorter lengths. This was accomplished by carrying out ultrasonication of the nanobelts in absolute ethanol, thereby suspending them in the liquid. During the DEP experiments it was found that the lengths of the vast majority of the suspended nanobelts were in the 10's of micrometers. However, some very short nanobelts with lengths of a few micrometers (typically 1−2 μm) were also present, which formed pearl chains.[29]

Experimental Setup and Testing. Figure 2 shows a schematic of the experimental setup. The PDMS microchannel was aligned and attached over the gold microelectrode array (Figure 1c), forming the liquid chamber for the DEP experiments. Polyimide coated flexible fused silica capillary tubing of outer diameter ~250 μm, and inner diameter ~100 μm (Polymicro

(55) Dai, Z. R.; Pan, Z. W.; Wang, Z. L. *Adv. Funct. Mater.* **2003**, *13*, 9–24.

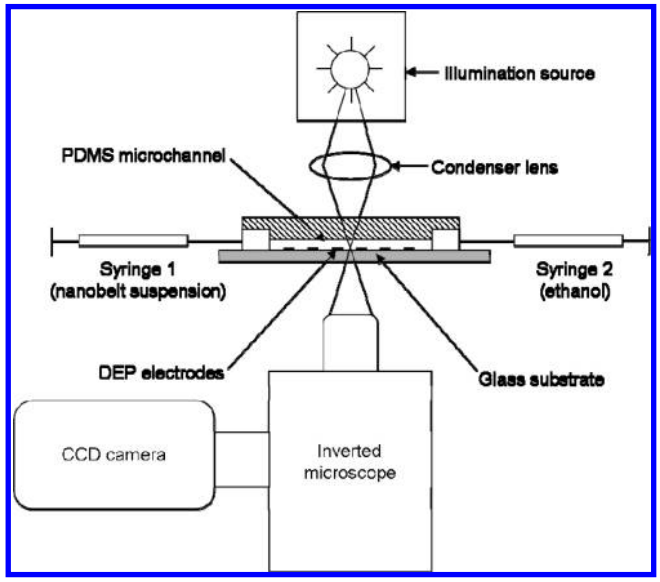

Figure 2. Schematic of the experimental setup used for imaging of dielectrophoresis induced nanobelt motion.

Technologies LLC, Phoenix, AZ) was used for delivery of the nanobelt suspension (or just ethanol) from a glass syringe to the PDMS microchannel. The syringe was fitted with a luer lock to capillary electrophoresis (CE) column adapter (InnovaQuartz, Inc., Phoenix, AZ) so that the capillary tube could have a leak free connection with the syringe. The ~250 μm diameter capillary tubes were connected to the inlet and exit (~250 μm square cross section) of the PDMS microchannel. One of the syringes was filled with SnO_2 nanobelt suspension in ethanol, and the other was filled with just ethanol liquid. The SnO_2 nanobelt suspension was introduced into the PDMS microchannel inlet by pressing the first syringe. One could slow down the nanobelts coming from the inlet side by pressing the other syringe connected to the exit, providing a better control of the location of the nanobelts to be studied in the ~10 μm tall central section (see Figure 1a) of the microchannel.

The electric field inside the microchannel was generated by applying ac voltage signals between the electrodes to induce DEP forces. A synthesized function generator (model DS345, Stanford Research Systems Inc., Sunnyvale, CA) in combination with a transformer was used for low- frequency (5 Hz−100 kHz) signals. A power amplifier/generator (model AG 1006 LF, T&C Power Conversion, Inc., Rochester, NY) was used as a source of rf signals in the high-frequency range (1−10 MHz). Since the DEP force depends on the volume of the particle[29] and nanobelts are very small,[1] large voltages (~70 V_{peak}) were required to observe the nanobelt motion clearly. Also, the large electrode gap size (~20 μm) made the use of large voltages necessary to establish significant electric field gradients. Because of the insulating nature of absolute ethanol, it was possible to avoid problems such as electrolytic dissociation and bubble formation in the microchannel even on application of such voltages.

The motion of the single nanobelts in the microchannel was observed using an inverted optical microscope (Nikon Eclipse TE2000-S, Nikon Instruments Inc., Melville, NY) coupled with a digital CCD camera for image acquisition. Proper lighting is critical for good imaging of small structures like nanobelts. Hence, a condenser (lens) with 0.3 NA (TE-C ELWD, Nikon Instruments Inc., Lewisville, TX) was used with the microscope for illumination of the DEP electrode chip and improved imaging. Digital images and movies were acquired using a computer controlled imaging software (MetaMorph Imaging System, version 5.0, Universal Imaging Corporation, Downingtown, PA), which enabled automated image capture and analysis from the digital CCD camera. Proper adjustments of the brightness and contrast settings in the software enabled clear visualization of the nanobelts. In fact, nanobelts of width as narrow as ~100 nm could be detected by utilizing the Köhler illumination[56] technique with the condenser and by adjusting the brightness and contrast settings. Köhler illumination helps in achieving the best optical resolution possible in a light microscope. By adjusting the size of the imaging regions in the software, movies with frame rates in the 15−25 fps (frames per second) range could be acquired. With full frame image acquisition, the frame rate was on the order of 10 fps.

RESULTS AND DISCUSSION

Positive Dielectrophoresis. In the megahertz frequency range of the applied electric field, positive DEP of the nanobelts was observed. Figure 3 is a sample from the measurements, which shows one of the ends of a nanobelt (dark line) gradually getting attracted toward the top electrode (dark cone). The other end of the nanobelt remained almost fixed in the lower electrode. The nanobelt was fixed to the lower electrode by attracting it from the nanobelt suspension. At the beginning of the experiment, the nanobelt suspension was allowed to flow into the channel. When the electric field was applied, the lower end of the nanobelt got attracted to the lower electrode due to positive DEP. Once the nanobelt got attracted to the electrode surface, the fluid did not affect the fixed end. The free end that was not touching any surface (the upper electrode or glass) could move if large fluid flow was induced. After the first end of the nanobelt got attracted to the lower electrode, flow of the suspension was stopped and the effect of positive DEP on the free end of the nanobelt was studied and recorded. The DEP force was found to be stronger than that of any residual fluid flow effects, if any. However, the attractive forces were much weaker compared to the repulsive forces (see the next paragraph), as can be observed from the longer time intervals for successive nanobelt positions in Figure 3 compared to Figure 4.

Negative Dielectrophoresis. Strong negative DEP (repulsion) of the nanobelts was observed in the low-frequency range (<100 kHz) range of the applied electric field. Figure 4 is a sample from the measurements, which shows the top end and the bottom end of the nanobelt getting repelled from the respective electrodes as a function of time. Because of the repulsion, the nanobelt rotated and ultimately became aligned along the central region of the microchannel. The strong force magnitudes can be appreciated from the short time intervals for the successive nanobelt positions in the figure. The nanobelt shown in Figures 3 and 4 are identical. It was first attracted and then repelled using voltage signals of different frequencies.

Nanobelt Deformation. For low-frequency (<100 kHz) voltage signals, the strong DEP forces caused deformation of the nanobelts. Parts a and b of Figure 5 are samples from the measurements at 50 kHz signal frequency, which shows the change in

(56) Köhler, A. In *Köhler Illumination Centenary*; Royal Microscopical Society: Oxford, U.K., 1994; pp 1−5.

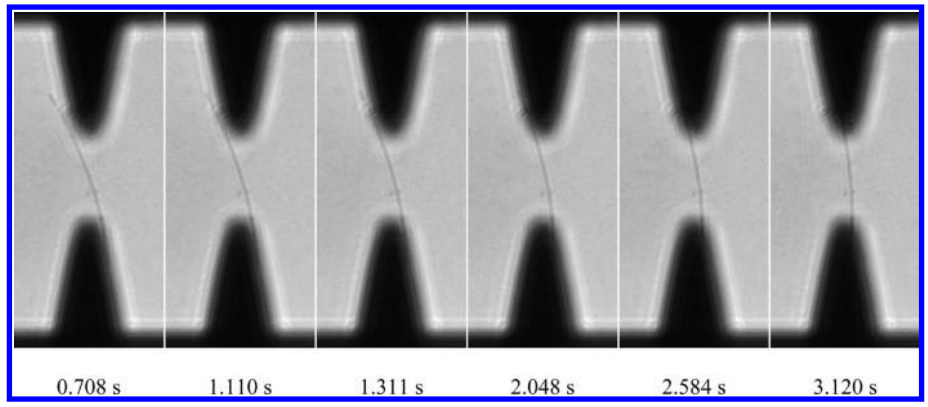

Figure 3. Time snapshot (from 15 fps movie) showing nanobelt attraction at a high-frequency voltage signal (70 V_{peak}, 10 MHz). The width of the nanobelt is estimated to be on the order of ~200 nm.

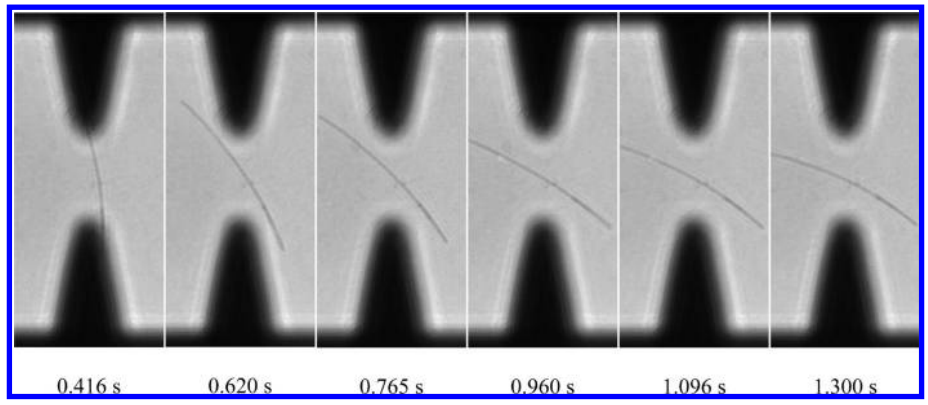

Figure 4. Time snapshot (from a 15 fps movie) showing nanobelt repulsion at a low-frequency voltage signal (70 V_{peak}, 50 kHz). The width of the nanobelt is estimated to be on the order of ~200 nm. This is the same nanobelt that is shown in Figure 3.

position and deformation of a long nanobelt due to the strong repulsive forces. For lower frequencies, the deformation was higher because of stronger DEP forces. In many situations, the nanobelts vibrated between the electrodes because of the interaction of the DEP force and the restoring force of the nanobelt due to its elastic nature. In the experimental result shown in Figure 5a, the two ends of the long nanobelt were fixed. For situations where the ends were not fixed, the repulsive forces caused the nanobelts to change position (rigid body motion). Some deformation was still seen in addition to the rigid body motion, although it was not as strong as in the case where the ends were fixed. Figure 5b shows the case when one of the nanobelt ends was fixed while the other was free. Under the influence of the repulsive forces due to negative DEP, the free end of the nanobelt vibrated and deformed since they are very flexible. The width of this nanobelt is much smaller compared to the one shown in Figure 5a.

While most of the images from the DEP experiments show the behavior of individual SnO_2 nanobelts, it is important to note that the reported DEP characteristics is representative of the nanobelt samples used in the experiments, in general. This was found to be the case by observing the individual nanobelts in real-time at different locations along the long microchannel, although it was not possible to record the motion of each and every nanobelt. However, on rare occasions multiple nanobelt behavior could be recorded as a function of time in a single field of view of the microscope. As evidence of the consistent DEP behavior of multiple nanobelts, a time snapshot of two nanobelts experiencing repulsion and deformation in the negative DEP regime is shown in Figure 6.

Pearl Chain Formation. The pearl chain formation[29] phenomenon refers to the end-to-end attachment of particles under the influence of electric fields resulting in an entity similar to that of a chain of pearls. A good description of the pearl chain formation mechanism is provided by Morgan et al.[30] For short nanobelts and particles, pearl chain formation was observed in the DEP experiments in the low-frequency range (<100 kHz) as well as in the high-frequency range (megahertz) of the electric field frequency. Parts a and b of Figure 7 show sample results from two separate DEP experiments in the low-frequency regime. The individual nanobelts and particles in the pearl chain are a few micrometers (typically 1−2 μm) in length/size. Figure 7a shows the situation when short nanobelts and particles aligned between the electrodes and formed a pearl chain, which then oscillated as a single entity between the electrodes. Figure 7b shows a slightly different situation compared to Figure 7a. The difference is that after the pearl chain formation, the chain also showed separation while still oscillating between the electrodes. To the best of our knowledge, this type of phenomenon has not been reported in the literature. Parts a and b of Figure 7 show a few time dependent positions of the pearl chain between the electrodes. It is believed that the oscillations between the electrodes are due to the influence of the restoring force on the particle chain. The origin of the restoring force is the repulsive DEP force which is position dependent and is highest near the two electrode edges and lowest in the central region between the electrodes. The force gradually

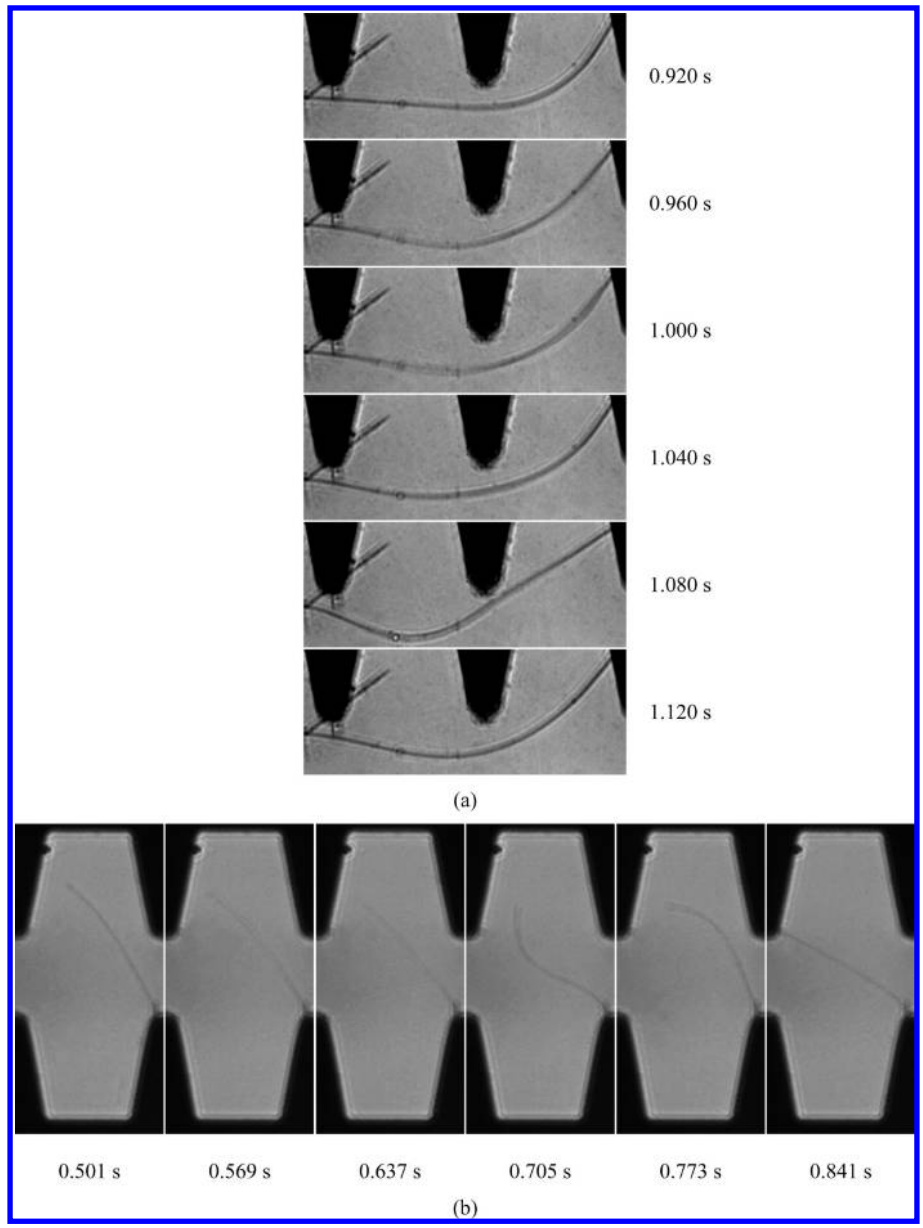

Figure 5. (a) Time snapshot (from a 25 fps movie) showing nanobelt deformation at a low-frequency voltage signal (87 V_{peak}, 50 kHz). Both ends of the long nanobelt are fixed. AFM measurement on this nanobelt after the experiment showed the thickness to be ~60 nm and width to be ~500 nm. The zigzag structure on the left electrode is another nanobelt which is connected to the long nanobelt (during the nanobelt growth). (b) Time snapshot (from a 15 fps movie) showing nanobelt deformation at a low-frequency signal (100 V_{peak}, 50 kHz). One end of the nanobelt is fixed while the other is free. The width of the nanobelt is estimated to be on the order of ~100 nm.

falls as the pearl chain moves from either electrode toward the central region. When the pearl chain comes near one of the electrodes, it is repelled strongly toward the central equilibrium position. The chain then overshoots this region and goes toward the other electrode. The other electrode repels the chain again toward the center. This motion continues as long as a low-frequency electric field is present between the electrodes. It was observed that sometimes the pearl chain became almost stationary in the central region between the electrodes. This is understandable since that position is an equilibrium position corresponding to a minimum DEP force magnitude. The reason for the separation of the pearl chain shown in Figure 7b is thought to be due to some amount of contact between the chain and the upper wall of the PDMS microchannel while moving between the two electrodes. This contact is possible because repulsive forces due to negative DEP on the chain causes it to move away from the electrodes, as well as above the glass surface. The surface contact induces friction forces and affects the equilibrium of the particles in the chain causing it to separate.

Pearl chain formation was also observed in the positive DEP regime (megahertz frequency). In the case of triangular electrodes, usually single pearl chains formed which aligned between the electrodes (just as in the case of the negative DEP regime), which then got attracted to one of the electrodes. In the case of castellated microelectrodes, formation of multiple pearl chains on single electrodes was observed, as shown in Figure 8. The pearl chain formations got attracted to the edges of the castellated electrodes. Because of the attractive DEP forces, the pearl chains did not oscillate as in the case of DEP in the low-frequency range. It can be observed that for most of the electrodes shown in the

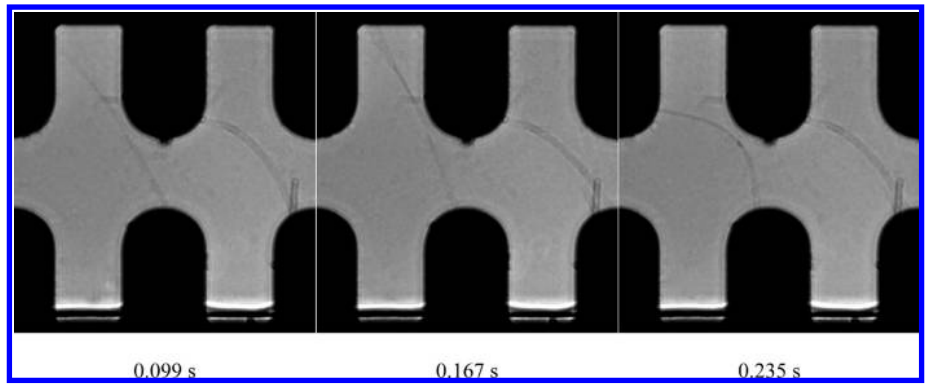

Figure 6. Time snapshot (from a 15 fps movie) showing repulsion and deformation of multiple nanobelts (the two dark curves) under the influence of negative DEP at a low-frequency voltage signal (87 V_{peak}, 50 kHz). The minimum gap between the semicircular gold microelectrodes (dark regions) is ~20 μm. The left nanobelt is experiencing position change and large deformations. In these image frames, the right nanobelt is experiencing small deformations which can be noted by the position change of its lower end, although earlier frames (not shown) indicated larger deformations. The short dark line in the vertical position sticking out of the lower right electrode is part of a nanobelt lying on top of the electrode surface and is not moving.

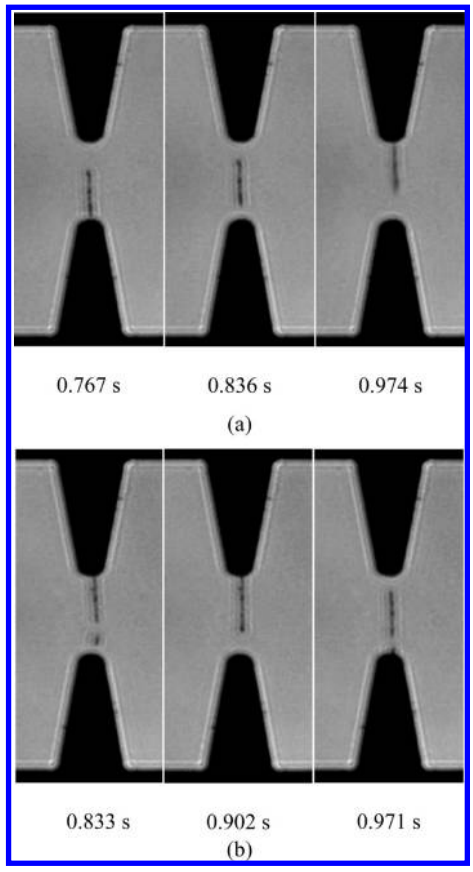

Figure 7. Time snapshot (from a 15 fps movie) showing (a) pearl chain formation of short nanobelts and particles into a single entity and (b) pearl chain formation and separation of short nanobelts and particles. The individual nanobelts/particles are a few micrometers (typically 1−2 μm) in length/size. The pearl chains oscillated between the electrodes due to negative DEP at 70 V_{peak}, 50 kHz voltage signal.

figure, three sets of pearl chains formed. Two of the chains are located in the two corner regions and the third chain is located in the flat central region of the castellated electrode. This is due to the high electric field gradients in these regions.

Frequency Dependence of DEP Force and Torque Magnitudes. Estimation of the relative DEP force and torque magnitudes as a function of the electric field frequency in the negative DEP regime (frequency <100 kHz) was made using additional experimental data[54] on a nanobelt of ~10 μm length, ~300 nm width, and ~60 nm thickness. The "crossover frequency"[13] was found to be ~100 kHz. Because of journal page limitations, the details, which can be found in another reference,[54] are not presented here.

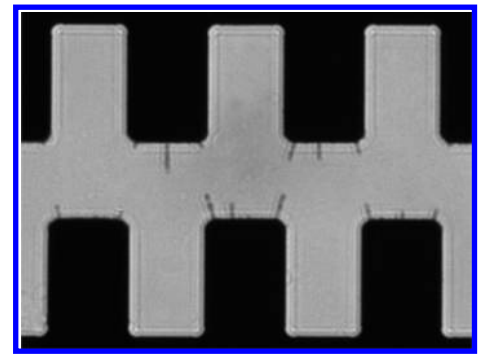

Figure 8. Image showing pearl chain formation of short nanobelts and particles on castellated gold microelectrodes due to positive DEP at ~40 V_{peak}, 10 MHz voltage signal. The individual nanobelts/particles are a few micrometers (typically 1−2 μm) in length/size. The minimum gap between the electrodes is ~20 μm.

Discussion of the Unusual DEP Characteristics. The presence of negative DEP in SnO_2 nanobelts in the low-frequency electric fields is unusual. The electrical conductivity of the absolute ethanol used for suspending the SnO_2 nanobelts in the experiments is on the order of 10^{-5}−10^{-4} S m^{-1}.[54] The measured average nanobelt electrical conductivity is on the order of 0.1 S m^{-1}.[54] Hence, the conductivity of the nanobelts was found to be always greater than that of ethanol. These conductivity values along with permittivity values from the literature were used to calculate the Clausius−Mossotti (CM) factor[29] discussed in the Theory section. It indicated that if nanobelts are treated as bulk material, with uniform dielectric properties, negative DEP is not possible for the frequency range studied experimentally. Numerical calculations[54] using the Maxwell stress tensor methodology[53] (applicable for general particle shapes) have also confirmed this finding. It was also found that in the low frequencies the electrical conductivities of the nanobelt and the liquid ethanol primarily determine the DEP force, while

the permittivities determine the DEP force in the high frequencies. This behavior is consistent with the basic polarization mechanisms involved in the dielectrophoresis phenomenon depending on the applied electric field frequency.[30] Hence, the most likely reason for the negative DEP is thought to be related to the presence of a nonconducting layer on the nanobelt surface. The presence of depletion layers on the surfaces of metal oxide semiconductors such as SnO_2 have been reported in the literature.[57] Conductivity can change orders of magnitudes in semiconducting materials due to effects such as depletion. While the possibility of permittivity change in nanostructures does exist to some degree, it is not likely to be in the orders of magnitude range. Hence, the effect of conductivity change is likely to determine the overall behavior of the nanobelt DEP in the low frequencies. The unusual DEP effect is investigated and explained through detailed numerical simulations[54] by including the effects of conductivity and permittivity change. Bulk type models and shell type models (with depletion layers on the nanobelt surfaces) are used to represent the nanobelt, and the resulting DEP characteristics are compared. While it is generally known that one cannot use bulk properties to characterize nanostructures, its likely manifestation in the DEP characteristics of nanostructures such as nanobelts is an important finding. Because of the unique aspect ratio of the nanobelt cross section (thin and wide rectangle), surface dominant effects are expected to play a much more important role in comparison with other types of nanowires.

CONCLUSIONS

An experimental setup was devised and fabricated to conduct detailed and direct real-time investigation of the DEP phenomenon in ethanol suspended SnO_2 nanobelts under ac electric fields over a wide frequency range (hertz to megahertz). The experiments performed on individual nanobelts revealed a wide variety of nanobelt motions under the electrically generated forces. These include attraction and repulsion, deformation of long nanobelts, and pearl chain formation of short nanobelts and particles. The existence of negative DEP phenomenon for electric fields in the low-frequency range is unusual. The most likely reason for this phenomenon is the presence of a nonconducting layer on the surface of the nanobelt. Because of the very small thickness of the nanobelt, the nonconducting layer can affect the dielectric properties (the electrical conductivity and possibly the permittivity) of the nanobelt as a whole, and hence modify the DEP characteristics. Details are presented elsewhere. Although the current research focused mainly on SnO_2 nanobelts, the insights gained from this study can be applied to other nanostructures in general and to nanowires and nanobelts of functional oxide materials in particular.

(57) Martinelli, G.; Carotta, M. C. *Sens. Actuators, B* **1995**, *23*, 157–161.

ACKNOWLEDGMENT

The authors wish to acknowledge the financial support of the Nanoscience and Nanotechnology Fellowship Committee of the Georgia Institute of Technology for providing funding for 1 year through a Nanoscience and Nanotechnology (NaST) Fellowship to the first author and the Georgia Tech Nanoscience/Nanoengineering Research Program for additional financial support. Thanks are also due to Prof. Martha A. Grover for providing funding for buying a condenser for the inverted optical microscope. Special thanks go to Dr. Xiangyang Kong for preparing the nanobelt sample and to the staff of the Microelectronics Research Center (MiRC) at Georgia Tech for the clean room facilities used for microfabrication.

Received for review June 21, 2009. Accepted January 19, 2010.

AC901287Z